Ashraq M. Kadim
Khalid H. Abass

Department of Physics,
College of Education for
Pure Sciences,
University of Babylon,
Hilla, IRAQ

Ag_2Se Nanoparticles Synthesis by Co-Precipitation Method: Characterization and Antimicrobial Evaluation

Silver selenide (Ag_2Se) nanoparticles possess promising optoelectronic properties, making them attractive for applications in biomedical fields such as bioimaging and biosensing. In this study, Ag_2Se NPs were successfully synthesized via the chemical co-precipitation method. Field emission scanning electron microscopy (FE-SEM) images revealed that the nanoparticles exhibited a tightly packed lamellar-like morphology with particle sizes 48nm. X-ray diffraction (XRD) analysis confirmed the formation of an orthorhombic β-phase structure of Ag_2Se. Energy-dispersive X-ray spectroscopy (EDX) confirmed the elemental composition, showing an atomic ratio of Ag to Se close to the ideal 2:1 stoichiometry. UV–visible spectroscopy showed a distinct absorption peak at 250 nm. The optical dispersion behavior was analyzed using the Wemple–DiDomenico single effective oscillator model, through which the refractive index dispersion, average oscillator energy (E_o), and dispersion energy (Ed) were determined. Additionally, the first-order (M-1) and third-order (M-3) spectral moments were calculated based on the extracted E_o and Ed values to further interpret the optical transitions. Beyond structural and optical characterization, the antibacterial activity of the synthesized Ag_2Se NPs was also evaluated. The results demonstrated notable antibacterial efficacy, indicating the potential of Ag_2Se nanomaterials for applications in medical, and environmental.

***Keywords*:** Silver selenide; Chemical coprecipitation; Antimicrobial activity; Bioimaging
Received: 27 April 2025; **Revised:** 5 June 2025; **Accepted:** 12 June 2025

1. Introduction

Over the past 20 years, because of their distinct size and structure, semiconductor nanocrystals have garnered a lot of interest. Because of their smaller size and greater surface area, nanoparticles have considerably better biological, chemical, and physical properties than micro-particles [1]. They are between 1 and 100 nm in size. Nanoparticles have several unique characteristics as a result of their enhanced surface reactivity [2]. Several important changes occur as microparticles migrate to nanoparticles. Surface area relative to volume has increased significantly, as have quantum phenomena [3]. The characteristics of the particle and its interactions with other materials are impacted by this process; the particles tend to accumulate since there are a lot more molecules or atoms on the surface than there are in the mass of the sample nanoparticles are naturally unstable due to enhanced van der Waals force on their surfaces, resulting in agglomeration [4-6]. Ag_2Se, also known as nominate, is a semiconductor substance that is rarely found naturally as a metal. It belongs to I-VI compounds [7]. Among semiconductor nano-materials, Ag_2Se nanoparticles are one of the most explored chalcogenide nano-materials due to their multiple uses, such as in the biomedical and electronics fields [8,9]. Ag_2Se nanoparticles is a MWIR CQD that has recently expanded the family of intraband CQDs and it is uniquely free of heavy metals. Because of their distinct electrical and optical characteristics that set them apart from their counterparts, Ag_2Se nanoparticles are among the most studied chalcogenide materials. They are perfect for use in thermoelectric circuits, semiconductors, and infrared detectors. In the realm of biomedicine, because of their high electrical conductivity and narrow band gap. Compared to other materials like CdSe or PbS, Ag_2Se quantum dots have a lower toxicity and can be used for deep-tissue imaging with better tissue penetration and higher resolution due to their emission in the second infrared region (NIR-II: 1000-1700nm) [10]. There are two different crystalline phases in which Ag_2Se nanoparticles can be produced. The orthorhombic crystal phase of β-Ag_2Se exhibits semiconductor behavior at low temperatures (0K). The space group P212121 is associated with the lattice parameters a = 4.33, b = 7.06, and c = 7.76 Å. It is a semiconductor that is n-type and has a tiny band gap. In contrast, the body-centered cubic (α-Ag_2Se) phase at high temperatures around 135°C (409K) exhibits metal-like properties [11].

Silver chalcogenides, especially Ag_2Se nanoparticles, are semiconductors with distinct physical properties [11-14]. Ag_2Se nanoparticles are prepared by several methods, including high-temperature heating of Ag and Se mixtures, microwave irradiation, and hydrothermal, electrochemical. Numerous investigations have looked at Ag_2Se nanoparticles various properties at the size of bulk forms, quantum dots, nano-structures, and microstructures [15-19]. Agar diffusion screening.

The antimicrobial activity of test materials is frequently assessed utilizing low-cost agar diffusion techniques such as agar plug, agar spot, well diffusion, and disc diffusion experiments. These methods depend on the antimicrobial substances dispersing into the surrounding agar medium through paper discs, wells, or plugs. This stops the bacteria that were injected from growing on the agar surface [20-22].

This study aims to synthesize and characterize Ag_2Se nanoparticles using the co-precipitation method. The proposed method offers a simple, cost-effective, and environmentally friendly route for Ag_2Se nanoparticles e synthesis, using Na_2SO_3 as a reducing agent for selenium. The process is important because it doesn't use toxic solvents or harsh reaction conditions. It also lets you control the size and distribution of the particles, making it a safer and more environmentally friendly alternative to traditional methods of synthesis. We used UV-visible spectroscopy, x-ray diffraction (XRD), field-emission scanning electron microscopy (FE-SEM), and energy-dispersive x-ray spectroscopy (EDX) to study the synthesized nanoparticles. They also looked at how well they killed germs, which showed how useful they could be in medicine and the environment.

2. Experimental Procedures

The chemicals used for the synthesis of Ag_2Se nanoparticles are sodium sulfite (Na_2SO_3) from Gainland Chemical (96% purity), silver nitrate ($AgNO_3$) from Daejung Chemicals (99.8% purity), and selenium (Se) from HPLC Company Ltd. (India, 99.7% purity). All of the chemicals used in this study are extremely pure and don't require any additional purification. The following are typical synthesis methods. The synthesis of Ag_2Se nanoparticles was carried out in three main stages. In the first stage, 3.14 g of Na_2SO_3 and 0.98 g of elemental selenium (Se) were dissolved in 50 mL of deionized water under constant stirring. The solution gradually changed in color from black to translucent, indicating the reduction of selenium (Se^0) to selenide ions (Se^{2-}) and the formation of sodium selenide (Na_2Se). In the second stage, 0.8 g of $AgNO_3$ was dissolved in 5 mL of deionized water to prepare the silver precursor solution. Subsequently, 5 mL portions of the previously prepared Na_2Se solution were added dropwise to the $AgNO_3$ solution under continuous stirring. This stepwise addition was repeated until the entire volume of Na_2Se was consumed. The gradual mixing facilitated controlled reaction kinetics and promoted the homogeneous formation of Ag_2Se nanoparticles. A distinct color change to black was observed, confirming the successful precipitation of Ag_2Se nanoparticles. In the final stage, the reaction mixture was stirred for an additional 30 minutes to ensure completion of the synthesis process. The resulting Ag_2Se nanoparticles were then separated by centrifugation at 3000 rpm for 15 minutes. The collected precipitate was washed six times with ethanol and deionized water to remove residual salts and impurities. Particle agglomeration was effectively reduced by careful stirring, the gradual addition of Na_2Se to $AgNO_3$, and repeated centrifugation with washing. These steps contributed to a homogeneous distribution of nanoparticles without the need for chemical stabilizers. Finally, the purified Ag_2Se nanoparticles were dried in an oven at 80 °C for three hours.

CuKα radiation was used to record XRD patterns using a Spectris Analytical X-ray diffractometer. FE-SEM was used to introduce the sample's surface morphology, while the chemical constitution and purity of the prepared Ag_2Se nanoparticles were examined by EDX. UV-visible spectroscopy was performed with a Shimadzu UV1800 spectrophotometer. At room temperature, the measurements were made in the wavelength range of 200-800 nm. To perform the analyses, the samples were placed in quartz cuvette cells of 1 cm path length.

3. Results and Discussion

XRD was used to examine the phases and crystal structures of the prepared nanoparticles and their patterns are shown in Fig. (1). They contain distinctive peaks that are similar to the orthorhombic Ag_2Se β-phase. This matches the JCPDS card no. 024-1041, which is the naumannite.

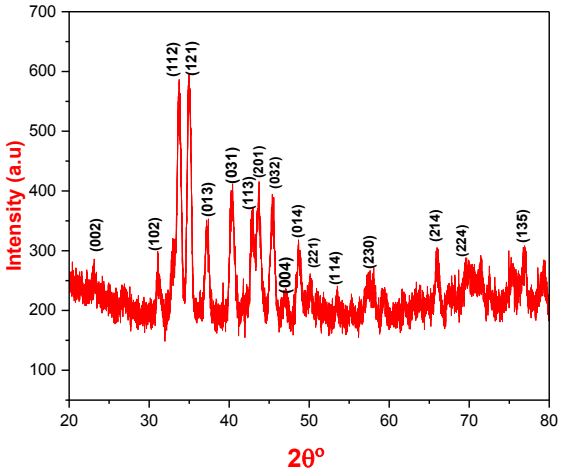

Fig. (1) XRD pattern of Ag_2Se NPs

The XRD pattern showed no undesirable phases corresponding to any secondary structures, confirming the purity of the products. The crystalline nature of the Ag_2Se nanoparticles was verified by the presence of distinct diffraction peaks. The broadening of these XRD peaks can be attributed to two main factors: the small crystallite size and internal lattice strain. While the reduced size contributes to peak broadening, the strain within the crystal lattice leads to both peak

broadening and slight shifts in position. Consequently, the peak width reflects the combined influence of these two factors, as illustrated in Fig. (1). This broadening is generally categorized into two types: mechanical broadening and physical broadening. The following relation yields the revised instrumental broadening as shown in Eq. (1) [23,24]:

$$(\beta_D)^2 = (\beta_m)^2 - (\beta_i)^2 \quad (1)$$

where β_i represents the instrumental broadening, β_m represents the measured broadening, and β_D represents the corrected broadening. FWHM is used to quantify the sample's physical and instrumental widening. The Scherrer's equation can be used to determine the average crystallite size using modified physical broadening as shown in Eq. (2).

$$D = \frac{k\lambda}{\beta cos\theta} = \frac{0.9\lambda}{\beta cos\theta} \quad (2)$$

where λ is the x-ray wavelength, β is the FWHM, and θ is the Bragg's angle. The lattice parameters were derived using the following relationship [25]:

$$\frac{1}{d_{hkl}^2} = \frac{h^2}{a^2} + \frac{k^2}{b^2} + \frac{l^2}{c^2} \quad (3)$$

where hkl stands for the Miller indices and d_{hkl} for the interplanar spacing. Table (1) lists all parameters that were calculated using the XRD data. Based on the Debye-Scherrer formula, the produced Ag_2Se nanoparticles had an average crystallite size of 16.92 nm, were several peaks are used to calculate the crystal size using the Scherrer's equation, and the average is then taken.

Table (1) Structural parameters of Ag_2Se NPs

Pos. [°2θ]	(hkl)	d-spacing [Å]	Height [cts]	FWHM	D
231314	(002)	3.31546	11.96	0.5622	14.53
31.1538	(120)	2.86856	35.07	0.5821	14.17
33.9004	(112)	2.70358	52.06	0.9079	9.14
34.8553	(121)	2,57194	211.36	0.3452	24.12
37.206	(013)	2.41466	99.5	0.5455	18.40
40.3403	(031)	2.23398	134.2	0.6482	13.06
42.8665	(113)	2.108	103.72	0.5099	16.74
43.6597	(201)	2.07152	119.18	0.6476	13.22
45.3752	(032)	1.99711	116.33	0.6266	13.74
46.9676	(004)	1.93305	20.02	0.4959	18.85
48.6805	(014)	1.86896	63.93	0.6347	13.55
50.0515	(221)	1.82093	31.97	0.5879	19.15
53.4388	(114)	1.71322	14.9	0.2663	33.40
57.6384	(231)	1.55782	13.3	0.3255	26.56
65.93	(214)	1.41566	45.36	0.5121	18.49
70.2872	(004)	1.33819	31.95	2.5235	3.85
76.7736	(134)	1.24048	45.36	0.613	16.53

The FE-SEM images of Ag_2Se nanoparticles at different magnifications, shown in Fig. (2a–c), reveal that the sample consists of small nanoparticles less than 100 nm with a homogeneous and densely packed lamellar-like morphology. In particular, figure (2c) shows smaller nanoparticles surrounding larger ones, as indicated by the red circles, clearly illustrating the aggregation behavior. The particle size distribution was quantitatively analyzed using ImageJ software.

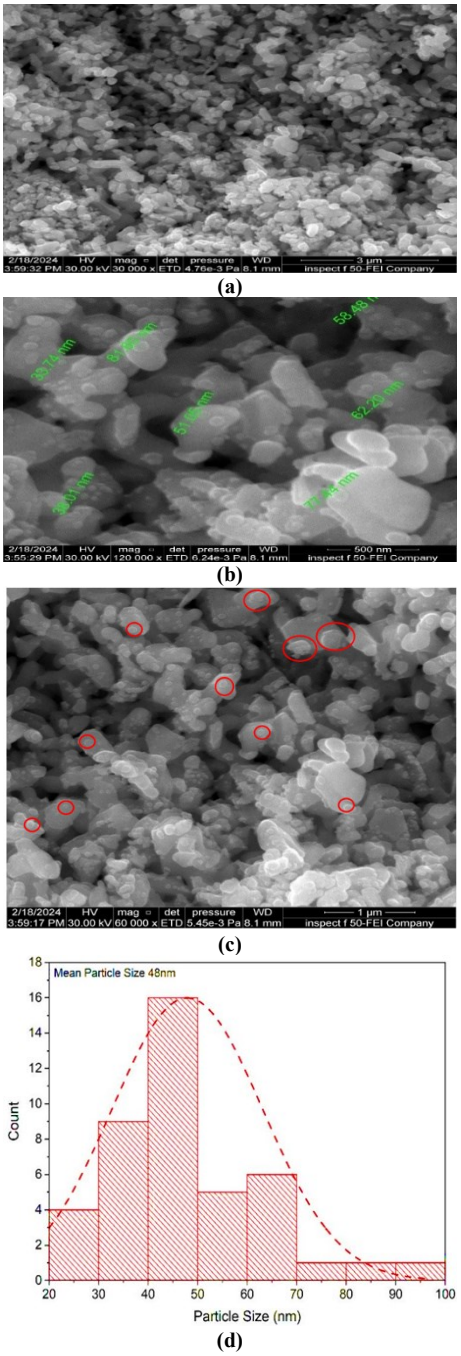

Fig. (2) FE-SEM images (a, b, and c at different magnification), (d) histogram of particle size of Ag_2Se NPs

Figure (2d) shows a histogram of the particle size of Ag_2Se nanoparticles. It was found that the mean particle size is 48 nm [26]. One of the primary challenges during the synthesis was preventing nanoparticle agglomeration. Agglomeration of Ag_2Se nanoparticles was minimized by carefully controlling the stirring speed and duration, along with repeated centrifugation and washing with ethanol and deionized water (six cycles). This process effectively removed impurities and ensured a uniform particle distribution without the need for chemical stabilizing agents.

Another key challenge was maintaining the precise stoichiometric ratio of Ag^{+} to Se^{2-} during synthesis to ensure the formation of pure-phase Ag_2Se nanoparticles.

The composition and purity of the synthesized Ag_2Se nanoparticles were analyzed using EDX spectroscopy at certain regions of the SEM pictures as shown in Fig. (3). This image shows the characteristic peaks of Ag_2Se nanoparticles, as well as their elemental compositions. The main emission energy line of Se was found in the 1.3–1.4 keV range, whereas that of Ag was discovered in the range of 2.8 to 3.0 keV, which in both instances is equivalent to the L-α peak of these two elements. Furthermore, dividing the silver peak intensity by the selenium peak intensity gives a ratio of 2:1, indicating the chemical formula Ag_2Se nanoparticles.

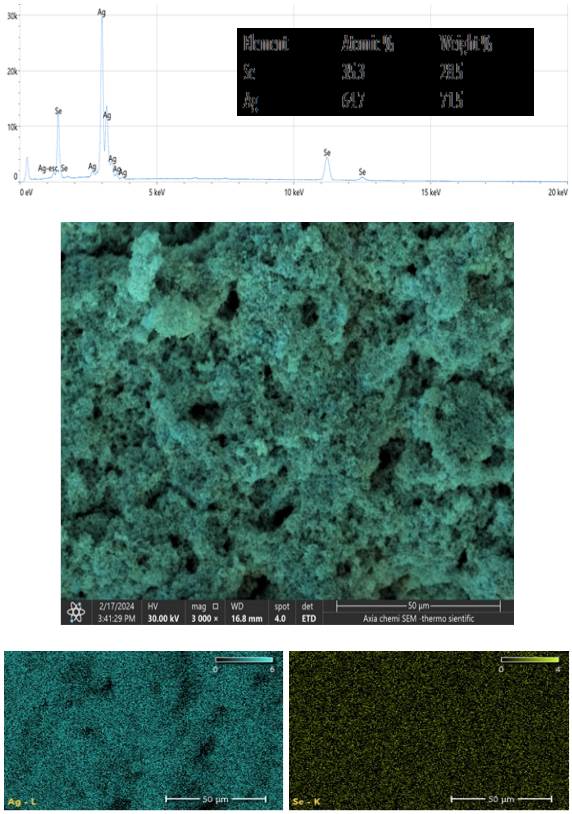

Fig. (3) EDX spectrum mapping of the elemental distributions of Ag and Se in Ag_2Se nanoparticle sample

Based on the EDX results, the atomic ratio of Ag (64.7%) to Se (35.3%) closely matches the stoichiometry of silver selenide (Ag_2Se), confirming the successful formation of the compound. The elemental color mapping of the Ag_2Se nanoparticles shows the homogeneity of the particles, supporting the uniform distribution of silver and selenium. The EDX spectra of the as-produced formulations showed no nitrogen peaks. This indicates the absence of any detectable traces of $AgNO_3$ ions. No other peaks associated with any impurities were observed in the EDX. This confirms the purity of the nanoparticles. These peaks observed in the spectrum are consistent with those previously identified [25,26].

The UV-visible spectra of Ag_2Se nanoparticles are displayed in Fig. (4). The absorption band ranges from 200 to 400 nm, with a maximum of approximately 250 nm. The sharp absorption peak indicates strong absorption due to the band gap transition rather than impurities [27-32]. Additionally, by serving as electron acceptors, facilitating charge transfer, pressing the Fermi level into the conduction band, and enhancing charge separation, oxygen vacancies in nanoparticles enhance absorption.

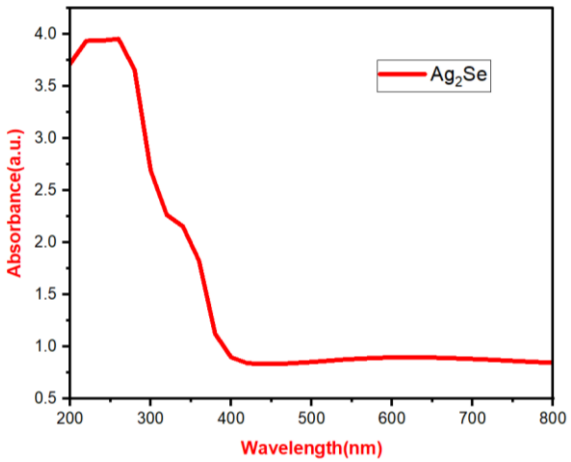

Fig. (4) UV–visible absorption spectrum of Ag_2Se NPs

The dispersion is a crucial component that must be taken into consideration when choosing materials for prospective uses or optoelectronic device designs that utilize spectral dispersion. The most effective model for examining these characteristics is the Single Effective Oscillator Model (EOM). The refractive index (n) to the effective single oscillator energies (E_o) and dispersion or strength energies (E_d) can be found using the following formula as shown in Eq. (4) [33-36]

$$(n^2 - 1) = \frac{E_d E_o}{[E_o^2 - (h\nu)^2]} \qquad (4)$$

Rearranging this equation to get Eq. (5) [36]:

$$(n^2 - 1)^{-1} = \frac{E_o^2 - (h\nu)^2}{E_d E_o} = \frac{E_o}{E_d} - \frac{(h\lambda)^2}{E_d E_o} \qquad (5)$$

A plot of $(n^2\text{-}1)^{-1}$ versus $(h\nu)^2$ shown in Fig. (5) produces a straight line in the linear region, from which the slope and y-intercept are extracted. In the fitted data, the slope was found to be 0.01, which corresponds to:

E_d = 1/slope = 1/0.01 = 100 eV

The y-intercept of the plot corresponds to $1/E_o^2$, and was determined as 1/28, yielding as shown in:

$$E_o = \sqrt{28} \approx 5.29 \text{ eV}$$

These values (E_o and E_d) were then used to calculate other important optical constants. For

example, the static refractive index (n_0) was determined using Eq. (6)

$$n_o = (1 + \frac{E_d}{E_o})^{\frac{1}{2}} \quad (6)$$

Additionally, E_o and E_d were verified using spectral moment calculations, as shown in equations (7) and (8):

$$E_o^2 = \frac{M_{-1}}{M_{-3}} \quad (7)$$

$$E_d^2 = \frac{M_{-1}^3}{M_{-3}} \quad (8)$$

Thus, the slope extracted from the fitted line in the dispersion plot plays a foundational role in determining the dispersion energy (E_d), which, in turn, is critical for evaluating optical behavior, polarizability, and designing optoelectronic devices based on the material [34-35].

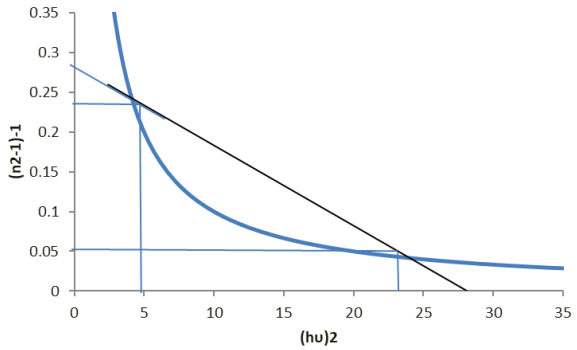

Fig. (5) Plot of $(n^2-1)^{-1}$ with $(hv)^2$ for Ag_2Se NPs

Table (2) Some important optical characteristics that were estimated for the Ag_2Se NPs

Slope	0.01
E_oE_d	100
E_o^2	28
E_o	5.291502622
E_g	2.645751311
E_d	18.89822365
$n^2(0)$	4.571428571
$n_o(0)$	2.138089935
ε	4.571428571
M_{-1}	3.571428571
M_{-3}	0.12755102

Using the agar well diffusion method, the antibacterial activity of Ag_2Se nanoparticles was assessed. To test the efficacy against *P. aeruginosa* and *E. faecalis*, Mueller-Hinton (MH) medium was distributed into sterile Petri dishes, and 20 mL of the medium was added to a liter of distilled water and heated with continuous stirring. Then, using sterile instruments, 6-mm-diameter wells were made in the agar medium, and various quantities of Ag_2Se nanoparticles (12.5, 25, 50, 100 µg/mL) were introduced to the wells. After that, the plates with the samples and microbes were incubated for 24 hours at 37°C. To ensure sterility, the MH medium was autoclaved at 121°C for 15 min. All the results of antibacterial activity at different concentrations are shown in figures (6) and (7), and in table (3). Manifested the inhibition zone in *P. aeruginosa* is higher than in *E. faecalis*, which shows an inhibition zone against *P. aeruginosa* was 24 mm, while it was 13 mm against *E. faecalis*. The difference in the effectiveness of Ag_2Se nanoparticles is attributed to the difference in cell wall composition between Gram-positive and Gram-negative bacteria, with *P. aeruginosa* being more susceptible due to its thin wall. *E. faecalis* may also possess defense mechanisms that reduce the effectiveness of the particles. Therefore, it is likely that these biological and physiological differences between the two strains are what causes the disparity in inhibition zones. These activities increased with an increased concentration for both type of bacteria, therefore the Ag_2Se nanoparticles are recommended as an Anti-bacterial material [37-39].

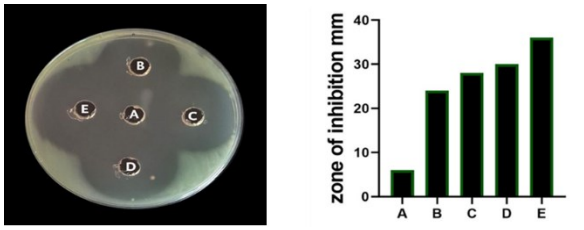

Fig. (6) Antimicrobial studies of various concentrations of Ag_2Se NPs against *P. aeruginosa* (A) control, (B) 12.5 µg/mL, (C) 25 µg/mL, (D) 50 µg/mL, and (E) 100 µg/mL

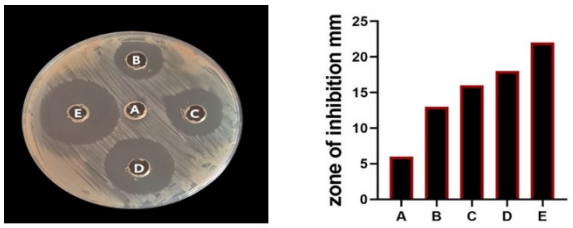

Fig. (7) Antimicrobial studies of various concentrations of Ag_2Se NPs against *E. faecalis* (A) control, (B) 12.5 µg/mL, (C) 25 µg/mL, (D) 50 µg/mL, and (E) 100 µg/mL

Table (3) The antimicrobial properties of Ag_2Se NPs

Antibacterial analysis (Zone of inhibition (mm)					
Sample	A	B	C	D	E
P. aeruginosa	6	24	28	30	36
E. faecalis	6	13	16	18	22

4. Conclusion

Ag_2Se nanoparticles were successfully synthesized using a simple and cost-effective co-precipitation method, yielding nanoparticles with good morphological and optical quality. This high quality can be attributed to the controlled reaction conditions of the co-precipitation process, which facilitated the formation of uniformly sized and well-dispersed nanoparticles. The moderate reaction rate, absence of secondary phases, and the purity of the precursors all contributed to producing highly crystalline and defect-free nanoparticles, leading to enhanced optical

behavior and a homogeneous morphology. The high purity of the Ag_2Se nanoparticles was confirmed, with no detectable impurities. These nanoparticles exhibited a homogeneous size distribution, with an average particle size of approximately 48 nm. The optical properties showed a strong absorption band around 250 nm. The Wemple-DiDomenico single-oscillator model provided a good description of the refractive index dispersion. Finally, the synthesized Ag_2Se nanoparticles demonstrated excellent antibacterial activity, indicating their potential for biomedical applications.

References

[1] P.N. Sibiya and M.J. Moloto, "Effect of Precursor Concentration and pH on the Shape and Size of Starch Capped Silver Selenide (Ag_2Se) Nanoparticles", *Chalcogen. Lett.*, 11(11) (2014) 577-588.

[2] E. Tarani et al., "Effect of ball milling time on the formation and thermal properties of Ag_2Se and Cu_2Se compounds", *J. Therm. Anal. Calorim.*, 148(23) (2023) 13065-13081.

[3] H.M. Ali and I.H. Khudayer, "Study structure and optical properties of Ag_2Se, $Ag_2Se_{0.8}Te_{0.2}$ and $Ag_2Se_{0.8}S_{0.2}$ thin films", *J. Ovonic Res.*, 18 (2022) 675-680.

[4] S. U. D. Wani et al., "A review on nanoparticles categorization, characterization and applications in drug delivery systems", *Vib. Spectrosc.*, 121 (2022) 103407.

[5] F. Eker et al., "A comprehensive review of nanoparticles: from classification to application and toxicity", *Molecules*, 29(15) (2024) 3482.

[6] S.B. Manjunatha, D.P. Biradar and Y.R. Aladakatti, "Nanotechnology and its applications in agriculture: A review", *J. Farm Sci.*, 29(1) (20166) 1-13.

[7] D.W. Ayele, "A facile one-pot synthesis and characterization of Ag_2Se nanoparticles at low temperature", *Egypt. J. Basic Appl. Sci.*, 3(2) (2016) 149-154.

[8] U.M. Chougale et al., "Synthesis, characterization and surface deformation study of nanocrystalline Ag_2Se thin films", *Mater. Phys. Mech.*, 17(1) (2013) 47-58.

[9] N. Singh et al., "A wide solar spectrum light harvesting Ag_2Se quantum dot-sensitized porous TiO_2 nanofibers as photoanode for high-performance QDSC", *J. Nanoparticle Res.*, 21 (2019) 1-10.

[10] S. Bin Hafiz et al., "Ligand engineering of mid-infrared Ag_2Se colloidal quantum dots", *Physica E: Low-dimen. Syst. Nanostruct.*, 124 (2020) 114223.

[11] O.G. Ozdal, "Green synthesis of Ag, Se, and Ag_2Se nanoparticles by Pseudomonas aeruginosa: characterization and their biological and photocatalytic applications", *Folia Microbiol. (Praha).*, 69(3) (2024) 625-638.

[12] S.-Y. Zhang et al., "Synthesis and electrochemical behavior of crystalline Ag_2Se nanotubes", *J. Phys. Chem. C*, 111(11) (2007) 4168–4174.

[13] V.D. Das and D. Karunakaran, "Variations of energy gap, resistivity, and temperature coefficient of resistivity in annealed β-Ag_2Se thin films", *Phys. Rev. B*, 39(15) (1989) 10872.

[14] Y. Cui et al., "Solvothermal syntheses of β-Ag_2Se crystals with novel morphologies", *J. Solid State Chem.*, 172(1) (2003) 17-21.

[15] W. Wang et al., "A novel room temperature method to nanocrystalline Ag_2Se", *Mater. Res. Bull.*, 34(6) (1999) 877-882.

[16] Q. Cao et al., "Crystal defect-mediated band-gap engineering: a new strategy for tuning the optical properties of Ag_2Se quantum dots toward enhanced hydrogen evolution performance", *J. Mater. Chem. A,* 3(40) (2015) 20051-20055.

[17] J. Hu et al., "Hydrothermal growth of β-Ag_2Se tubular crystals", *Chem. Commun.*, 8 (2000) 715–716.

[18] W. Mi et al., "Thermoelectric transport of Se-rich Ag_2Se in normal phases and phase transitions", *Appl. Phys. Lett.*, 104(13) (2014) 133903.

[19] S. Mishra et al., "A Facile Molecular Precursor-based Synthesis of Ag_2Se Nanoparticles and Its Composites with TiO_2 for Enhanced Photocatalytic Activity", *Chem. Asian J.*, 11(11) (2016) 1658–1663.

[20] B.C. Mohanty et al., "Characterization of silver selenide thin films grown on Cr-covered Si substrates", *Surf. Interface Anal.*, 41(3) (2009) 170–178.

[21] M. Jafari, M. Salavati-Niasari and F. Mohandes, "Synthesis and characterization of silver selenide nanoparticles via a facile sonochemical route starting from a novel inorganic precursor", *J. Inorg. Organomet. Polym. Mater.*, 23 (2013) 357-364.

[22] D. Yang et al., "Facile room temperature solventless synthesis of high thermoelectric performance Ag_2Se via a dissociative adsorption reaction", *J. Mater. Chem. A*, 5(44) (2017) 23243-23251.

[23] M.S. Shirazi et al., "Very rapid synthesis of highly efficient and biocompatible Ag_2Se QD phytocatalysts using ultrasonic irradiation for aqueous/sustainable reduction of toxic nitroarenes to anilines with excellent yield/selectivity at room temperature", *Ultrason. Sonochem.*, 87 (2022) 106037.

[24] E. Atkins, "Elements of X-ray Diffraction", *Phys. Bull.*, 29(12) (1978) 572.

[25] A. Jasim et al., "A New Decentralized Robust

Secondary Control for Smart Islanded Microgrids", *Sensors*, 22 (2022) 8709.

[26] A. Ali and W.-C. Oh, "Preparation of Ag_2Se-Graphene-TiO_2 Nanocomposite and its Photocatalytic Degradation (RhB)", *J. Korean Ceram. Soc.*, 54(5) (2017) 388-394.

[27] L. Li et al., "Ag as cocatalyst and electron-hole medium in CeO_2 QDs/Ag/Ag_2Se Z-scheme heterojunction enhanced the photo-electrocatalytic properties of the photoelectrode", *Nanomater.*, 10(2) (2020) 253.

[28] C. Zeng et al., "Oriented attachment growth of ultra-long Ag_2Se crystalline nanowires via water evaporation-induced self-assembly", *Cryst. Eng. Comm*., 15(25) (2013) 5127–5133.

[29] K. Abdali et al., "Morphological, Optical, ElectricalCharacterizations and Anti-Escherichia coli Bacterial Efficiency (AECBE) of PVA/PAAm/PEO Polymer Blend Doped with Silver NPs.", *Nano Biomed. Eng.*, 14(2) (2022) 114-122.

[30] S.Z. Mirzaei et al., "Bio-inspired silver selenide nano-chalcogens using aqueous extract of Melilotus officinalis with biological activities", *Bioresour. Bioprocess.*, 8 (2021) 1-11.

[31] Y. Yue et al., "Solvothermal synthesis of micro-pillar shaped Ag_2Se and its thermoelectric potential", *Mater. Today Chem.*, 39 (2024) 102183.

[32] T. S. Lee et al., "The forming-free bipolar resistive switching characteristics of Ag_2Se thin film", *J. Phys. D: Appl. Phys.*, 50(20) (2017) 205103.

[33] S. Chand et al., "Morphological and optical study of Ag_2Se quantum dots", in *AIP Conf. Proc.*, 2009(1) (2018) 020026.

[34] A.M. Kadim et al., "Effect of loading corn starch nanoparticles on the morphological, optical, and dielectric behaviors of PVA/PMMA/PAAM polymer blend for optoelectronic and antibacterial applications", *Nano Biomed. Eng.*, 16(1) (2024) 119-127.

[35] A.S. Hassanien, R. Neffati and K.A. Aly, "Impact of Cd-addition upon optical properties and dispersion parameters of thermally evaporated $Cd_xZn_{1-x}Se$ films: discussions on bandgap engineering, conduction and valence band positions", *Optik*, 212 (2020) 164681.

[36] S.H. Wemple and M. DiDomenico, "Theory of the Elasto-Optic Effect in Nonmetallic Crystals", *Phys. Rev. B*, 1(1) (1970) 193-202.

[37] M.V.V. Prasad, K. Thyagarajan and B.R. Kumar, "Effect of Rotational Speed on Linear and Non-Linear Optical Properties of Sol-Gel Spin Coated Nanostructured CdS Thin Films", *J. Nanosci. Technol.*, (2019) 688-693.

[38] F. Hamood et al., "Preparation and Characterizations of PVA/Vanadium Nanocomposites for Gamma Ray Shielding and Antibacterial Activity Applications", *Int. J. Nanosci.*, 22 (2023) 00497.

[39] F. Hamood et al., "Effect of CdS Nanoparticles on Structural, Optical and Dielectric Properties for Gamma-Ray Shielding and Antibacterial Efficiency of PVA/PAAm Polymers Blend", *Int. J. Nanosci.*, vol. 22 (2023) 00436.

